Process Compensated Resonance Testing Modeling for Damage Evolution and Uncertainty Quantification

Eric Biedermann[2,a)], Julieanne Heffernan[2,b)], Alexander Mayes[2,c)], Garrett Gatewood[2,d)], Leanne Jauriqui[2,e)], Brent Goodlet[3,f)], Tresa Pollock[3,g)], Chris Torbet[3,h)], John C. Aldrin[4,i)], and Siamack Mazdiyasni[1,j)]

[1]*Air Force Research Laboratory (AFRL/RXCA), Wright-Patterson AFB, OH, USA*
[2]*Vibrant Corporation, Albuquerque, NM, USA*
[3] *University of California, Santa Barbara, Santa Barbara, CA, USA*
[4] *Computational Tools, Gurnee, IL, USA*

[a)] Corresponding author*:* ebiedermann@vibrantndt.com
[b)] jheffernan@vibrantndt.com
[c)] amayes@vibrantndt.com
[d)] ggatewood@vibranndt.com
[e)] ljauriqui@vibrantndt.com
[f)] bgoodlet@engineering.ucsb.edu
[g)] pollock@engineering.ucsb.edu
[h)] ctorbet@engineering.ucsb.edu
[i)] aldrin@computationaltools.com
[j)] siamack.mazdiyasni@us.af.mil

Abstract. Process Compensated Resonance Testing (PCRT) is a nondestructive evaluation (NDE) method based on the fundamentals of Resonant Ultrasound Spectroscopy (RUS). PCRT is used for material characterization, defect detection, process control and life monitoring of critical gas turbine engine and aircraft components. Forward modeling and model inversion for PCRT have the potential to greatly increase the method's material characterization capability while reducing its dependence on compiling a large population of physical resonance measurements. This paper presents progress on forward modeling studies for damage mechanisms and defects in common to structural materials for gas turbine engines. Finite element method (FEM) models of single crystal (SX) Ni-based superalloy Mar-M247 dog bones and Ti-6Al-4V cylindrical bars were created, and FEM modal analyses calculated the resonance frequencies for the samples in their baseline condition. Then the frequency effects of superalloy creep (high-temperature plastic deformation) and macroscopic texture (preferred crystallographic orientation of grains detrimental to fatigue properties) were evaluated. A PCRT sorting module for creep damage in Mar-M247 was trained with a virtual database made entirely of modeled design points. The sorting module demonstrated successful discrimination of design points with as little as 1% creep strain in the gauge section from a population of acceptable design points with a range of material and geometric variation. The resonance frequency effects of macro-scale texture in Ti-6Al-4V were quantified with forward models of cylinder samples. FEM-based model inversion was demonstrated for Mar-M247 bulk material properties and variations in crystallographic orientation. PCRT uncertainty quantification (UQ) was performed using Monte Carlo studies for Mar-M247 that quantified the overall uncertainty in resonance frequencies resulting from coupled variation in geometry, material properties, crystallographic orientation and creep damage. A model calibration process was also developed that evaluates inversion fitting to differences from a designated reference sample rather than absolute property values, yielding a reduction in fit error.

43rd Annual Review of Progress in Quantitative Nondestructive Evaluation, Volume 36
AIP Conf. Proc. 1806, 090005-1–090005-10; doi: 10.1063/1.4974649
Published by AIP Publishing. 978-0-7354-1474-7/$30.00

INTRODUCTION

Process Compensated Resonance Testing (PCRT) is a method for non-destructive evaluation (NDE) and material characterization that evaluates the ultrasonic resonance frequencies of a component. PCRT combines Resonant Ultrasound Spectroscopy (RUS) [1] with advanced pattern recognition algorithms and statistical scoring to perform PASS/FAIL NDE, process monitoring, life monitoring and material characterization for commercial applications [2]. Among the most critical of those applications are gas turbine engine blades made from Ni-based superalloys [3]. PCRT has demonstrated sensitivity to life-limiting material conditions caused by over-temperature exposure that reduce creep resistance of the material.

As turbine engines age and lose exhaust gas temperature margin, the combined temperature and stress on the airfoils eventually cause the airfoil microstructure to undergo changes resulting in a reduction of strength and creep resistance. Prior work on gas turbine airfoils exposed to high temperature and stress has shown that PCRT is capable of measuring consistent correlated shifts in resonance frequency peaks [3-4]. There is a critical need for quantitative models to more precisely relate these changes in the material state, with the resonance behavior of the material. It should be also recognized that in real engineered structures, multiple damage mechanisms often occur simultaneously, confounding the interpretation of the shift in resonance frequencies.

Building on prior research [5-8], this paper is focused on developing tools and techniques for PCRT forward modeling and model inversion with an emphasis on sensitivity to creep, microstructure representation, crystallographic orientation and uncertainty quantification. The goal is to more precisely connect changes in the resonance frequencies of gas turbine engine components to the component material and damage state, and to develop a robust PCRT material characterization capability.

PCRT MODELING

Recent research on PCRT modeling [5-8] has led to significant developments in forward modeling and model inversion techniques. figure 1 shows a diagram on forward modeling and model-based inversion in the PCRT context. A forward model takes what is known about the geometry and material state of a part to predict its resonance frequencies and mode shapes. Model inversion connects measured changes in resonance frequencies to a quantitative evaluation of the macro-scale test sample, micro-structure material state and ideally, life prediction. An inversion capability using surrogate models from finite element method (FEM) data has been developed. Compared to previous analytical inversion methods, FEM model inversion enables quantitative evaluation of crystallographic orientation, elastic properties, and parameters describing damage for complex geometries.

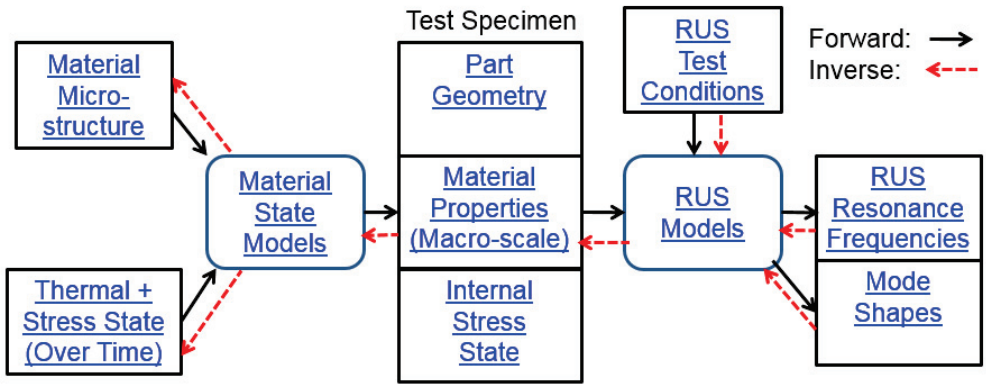

FIGURE 1. RUS forward modeling and model inversion

CREEP FORWARD MODELING

As detailed in [8] forward modeling efforts utilizing a relatively simple power-law hardening elastic-plastic constitutive law were shown to sufficiently capture the single dominant mechanism affecting resonance in polycrystalline (PX) MM247 dog bone samples crept from zero to 6.1% strain: uniform elongation of the gauge

section, i.e. the overall shape change associated with creep strain accumulation. After creep strain was increased (by one increment) to 8.8%, the measured dog bone sample used for FEM model verification exhibited substantial surface cracking along grain boundaries transverse to the applied load. These cracks were verified to be a secondary mechanism affecting resonance, only at high levels of creep strain accumulation, and only after the sample entered into a tertiary creep regime exhibiting an accelerated creep strain rate.

The studies detailed here apply creep damage forward modeling techniques to single crystal (SX) MM247. Figure 2 shows the deformation of an SX dog bone sample subjected to uniaxial tensile load. The [001] crystallographic orientation is the preferred crystal growth direction and is ideally aligned with the long axis of the sample. An FEM model of the dog bone was created, and constraints and loads were applied to simulate creep as described in [5], [6] and [8]. Within the model, the applied load was adjusted to produce varying levels of creep strains between 0.5% and 10% across the 10mm diameter gauge section of the dog bone.

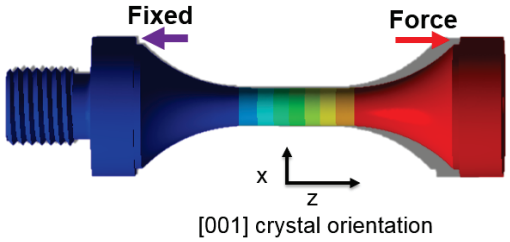

FIGURE 2. Example of uniaxial creep deformation in SX dog bone sample. The [001] crystallographic orientation is aligned with the long axis of the sample. Sample length = 50.4 mm

Modeling creep deformation in the cubic SX MM247 required an anisotropic elastic/plastic constitutive material model. For these creep damage studies, the Hill Stress Potential function [9] was used. After each creep strain interval was modeled, the deformed shape was imported into an ANSYS modal analysis to predict the change in resonance frequencies resulting from the shape change associated with the creep strain accumulation. The resonance frequencies for the crept model were then compared to the frequencies for the baseline geometry (figure 3), with care taken to ensure that the frequency comparisons were made between like mode. For this analysis, the angle between the [001] crystallographic orientation and dog bone long axis was also varied to capture the normal variation expected single crystal growth. Generally, creep damage causes a decrease in frequency in sensitive resonance modes. Results were consistent with [5], [6] and [8], where bending modes with significant deformation in the gauge section showed the largest frequency change. The effect of varying SX crystallographic orientation was an increase in the frequency splitting of degenerate bending modes.

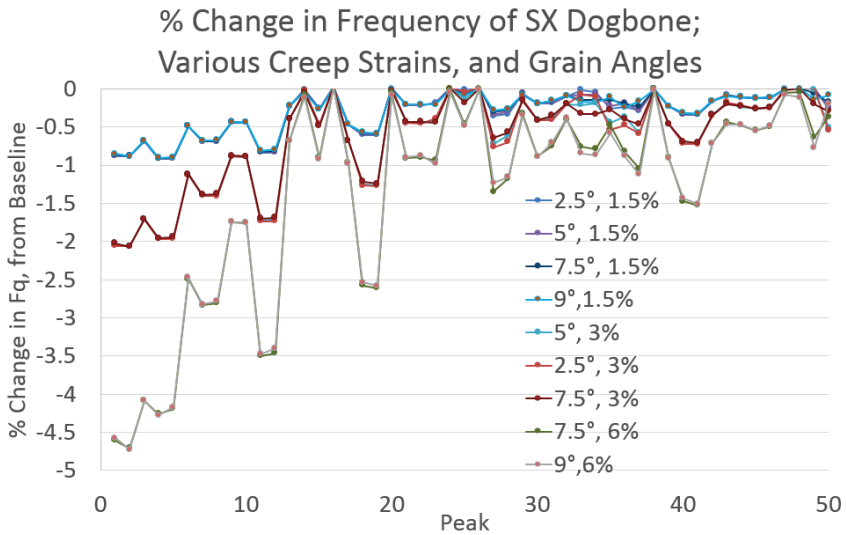

FIGURE 3. Percent frequency change for various creep strains, including grain angle effects

A major focus of the current PCRT modeling research is the development of virtual training sets with modeled design points that eliminate the need for large amounts of measured resonance spectra data that can be costly and difficult to obtain. Creep forward models were used to demonstrate the virtual training set capability. Modeled design points including only acceptable material property and geometric variation, as well as damaged model points reflecting a range of creep strain and the potential cracking that can result, were converted to virtual resonance spectra and imported into Vibrant's PCRT software.

Generation of candidate PCRT sorting modules followed the creation of the virtual database. The Vibrational Pattern Recognition (VIPR) algorithms were applied to the virtual training database to find the combination of resonance frequencies that were most effective at sorting crept components from acceptable components. In this creep study, a combination of four bending modes were identified as the most effective sorting module configuration, a result consistent with the creep parametric studies described above. Statistical scoring using the Mahalanobis-Taguchi System (MTS) calculated the Mahalanobis Distance between each component and the central tendencies of the known acceptable and crept populations. Limits were set for each criteria. Similarity to the acceptable population was evaluated with respect to the MTS limit. Similarity to the crept population was evaluated with respect to the Bias limit. For a part to pass the PCRT sort, it had to fall within both the MTS and Bias limits.

Figure 4 shows the PCRT Sorting Module plot. Parts in the lower left quadrant fall within the MTS and Bias limits and pass the sort. In the candidate sort shown, all of the parts in the acceptable population pass, as do the parts with 0.5% creep strain. As the absolute deformation from 0.5% creep strain was less than the gauge section length tolerance specified on the dog bone machining specification, this result was completely acceptable. All creep strains of 1.0% or greater failed the candidate sort.

The creep forward modeling tests demonstrated the effectiveness of creating PCRT sorting modules from virtual training sets of modeled design points. Future work will include verification and validation of the accuracy of those creep models and sorting modules. Verification results will be used for model and sort refinement.

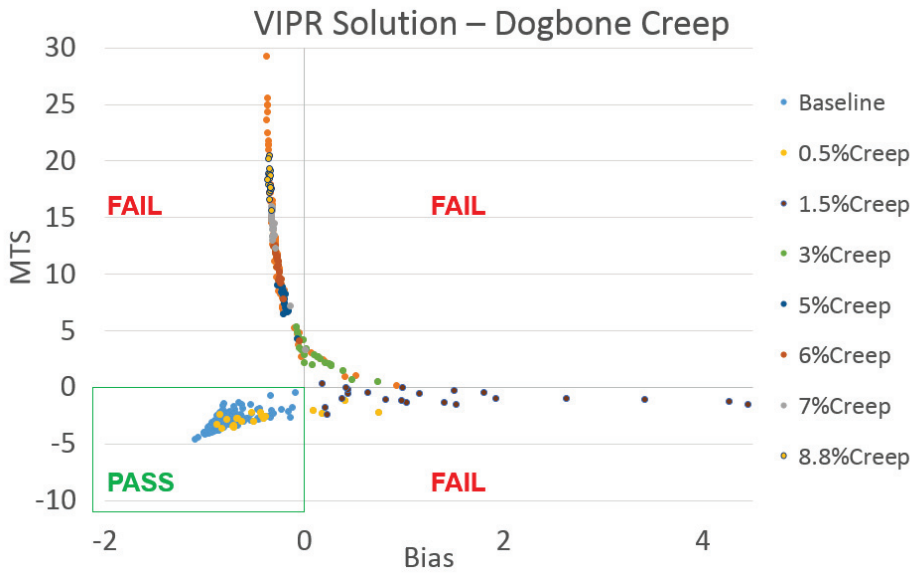

FIGURE 4. PCRT sorting results with virtual training set of acceptable components and components with creep strain

FORWARD MODELING OF TEXTURE IN TI-6-4

The scope of forward modeling studies has expanded to include simulations of the effects of texture in Ti-6Al-4V material. Ti-6-4 is used in several critical gas turbine engine applications, such as disks. Local volumes of material that possess a preferred crystallographic texture, known as microtexture regions (MTRs), are regions of hexagonal α-phase crystallites with a common crystallographic orientation with a combined size larger than primary α-phase grains [10]. MTRs have been shown to cause early fatigue failure in dwell fatigue conditions [10]. Yang et Al. [10]., define an orientation distribution function (ODF) as

$$F(\sigma,\theta) = F_0 \exp\left(\frac{\cos\theta}{2\sigma}\right) \quad (1)$$

and

$$F_0 = \frac{2S}{e^S - e^{-S}} \quad (2)$$

where σ is the texture parameter that governs the width of the orientation distribution function, and θ is the angle between the texture ideal direction and crystallographic orientation state and $S = 1/2\sigma$. The ODF describes the distribution of crystal orientations within the MTR with respect to σ. The ODF is used to weight the expression for the orientation volume average elastic stiffness tensor c_{ijkl}, given by [10]

$$\langle F c_{ijkl} \rangle = \frac{1}{8\pi^2} \int_0^{\pi} \int_0^{2\pi} \int_0^{2\pi} F(\beta,\alpha,\gamma) c_{ijkl} \times \sin(\beta) d\alpha d\gamma d\beta \quad (3)$$

where α, β, γ describe the crystallite orientation. The elastic constants for Ti-6-4 as a function of texture parameter were calculated, yielding the elastic stiffness vs. texture parameter values shown in figure 5 and table 1.

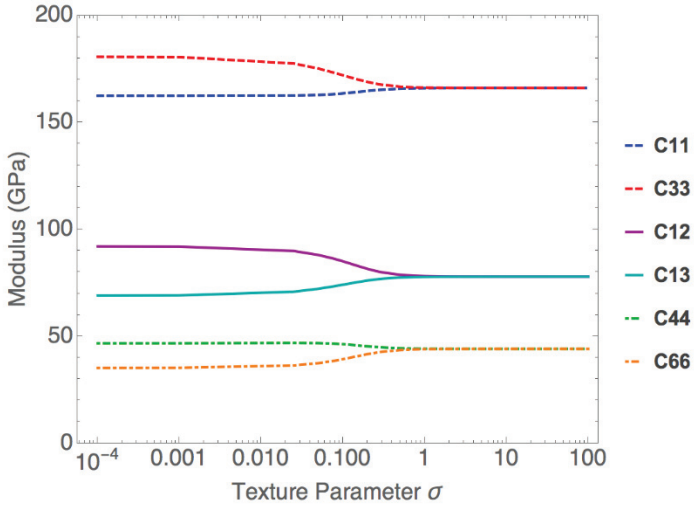

FIGURE 5. Plot elastic stiffness (C_{ij}) values for varying the texture parameter (σ) (right) for Ti-6-4

TABLE 1. Elastic stiffness (C_{ij}) for Ti-6-4 with variable texture parameter (σ), [units in GPa]

Designation:	**<----------More Hexagonal**				**Median**	**More Isotropic ----------->**			
Texture Parameter (σ):	**0.0001**	**0.05**	**0.09**	**0.12**	**0.14**	**0.2**	**0.5**	**1**	**10**
C11 = C22:	162.40	162.80	163.40	163.80	164.10	164.70	165.70	166.00	166.10
C12:	91.99	87.99	85.54	84.08	83.27	81.48	78.71	78.11	77.89
C13 = C23:	69.01	72.18	73.77	74.63	75.08	76.05	77.47	77.78	77.89
C33:	180.70	175.20	172.50	171.20	170.40	168.90	166.70	166.20	166.10
C44 = C55:	46.70	46.78	46.38	46.03	45.81	45.28	44.37	44.16	44.09
C66=(C11-C12)/2:	35.20	37.40	38.93	39.87	40.41	41.62	43.51	43.93	44.09

An FEM parametric study was run to determine the resonance frequency sensitivity to the various texture conditions in table 1. A cylinder was modeled in ANSYS, and a series of modal analyses were run with material properties set to the various elastic constants in table 1 to represent a 'macrotexture' condition applied to the entire sample. The σ=10 (fully isotropic) condition was set as the baseline condition. The frequency changes for the other

texture parameters were calculated with respect to this baseline. Figure 6 shows the results reflected an increase in material anisotropy with decreasing σ. Automated mode matching algorithms were applied to ensure that frequency change calculations compared the same modes. Extensional/breathing modes showed the greatest overall sensitivity, with changes in the positive direction on the order of 10% for the fully SX model (σ=0.0001). Torsional modes showed the greatest negative change, with changes on the order of -5.0%. Bending modes showed increasing degenerate peak splitting, with the splitting of some higher order degenerate modes large enough to span the x-axis (one mode showing a net increase in frequency while the other showed a net decrease).

The parametric studies presented here were a precursor for studies of more realistic MTRs. Future work will evaluate the effects of variation in the texture parameter, location, size, shape and crystal orientation of MTRs.

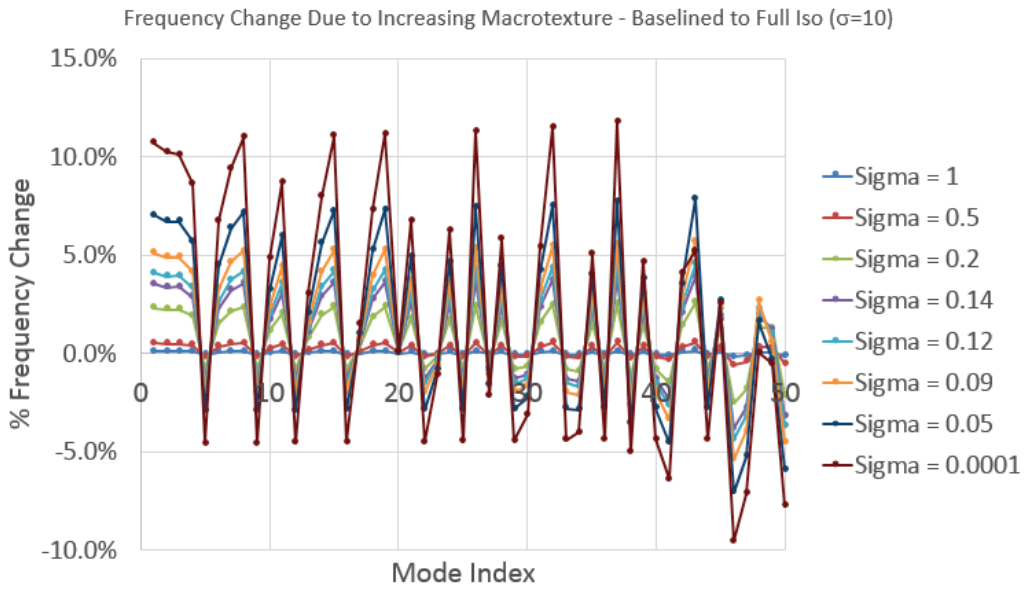

FIGURE 6. Frequency change vs. texture parameter applied to full cylinder, baselined to fully isotropic σ = 10 texture parameter

SINGLE CRYSTAL MAR-M-247 MATERIAL PROPERTY MODEL INVERSION

FEM-based PCRT model inversion introduces the potential to perform inversion for complex geometries and material damage/states. FEM-based model inversion begins with the generation of an FEM model "design space" representing the full range of possible combinations of model parameters as defined by the user. The design space is typically a gridded design of experiments (DOE) space that includes all combinations of input parameters within specified ranges and the resonance frequencies for each design point. Studies are also evaluating non-gridded 'meta-model' design spaces that use an n-dimensional function instead of discrete points, and iterative generation of FEM design points during inversion. Once the design spaces are defined, input frequencies are provided to the inversion algorithms, and the algorithms estimate the point in the design space that best fits the input through an iterative nonlinear least-squares scheme. Recent research addressed inversion studies for SX MM247 parallelepipeds with varying elastic material properties and crystal orientation in a gridded design space. The goal of these studies was to develop inversion approaches that can be expanded to more complex shapes and material states, including the effects of damage mechanisms like creep. Table 2 shows the parameters and value ranges in this study. Input parameters were the elastic modulus along the [001] crystallographic orientation (E_{001}), Poisson's Ratio along the [001] orientation (ν_{100}), the Zener anisotropy ratio (A) and the angle between the sample long axis and the [001] orientation (θ). Design space resolution was varied by adjusting the number of intermediate points between the min and max values.

TABLE 2. Model inversion parameter ranges

	Range	Min	Nominal	Max
E_{001}	+/- 2%	1.277x10^{11}GPa	1.303x10^{11} GPa	1.330 x10^{11} GPa
ν_{001}	+/- 7%	0.348	0.374	0.400
A	+/- 5%	2.615	2.753	2.890
θ	0-10°	0°	0°	10°

Examples of model inversion results for the medium resolution design space are shown in figure 7. In this study, four input resonance spectra were generated by FEM simulation runs to allow evaluation only of the inversion techniques, without measurement or model uncertainty. The tested inputs were made from parameters in-between the design space grid points, forcing the inversion algorithms to interpolate. Figure 7 shows the inversion result ("Est. Value") compared to the target ("Act. Value"), each starting with a randomized initial guess ("X0"). Horizontal lines indicate the gridded values ("Design Pts") and boundary values ("Bounds"). Each input was inverted three times, and all results were nearly 100% accurate. The accuracy of inversion fitting vs. design space resolution is shown in figure 8. The best fit results for E_{001} were compared for the low resolution and medium resolution spaces (81-point: three increments, 625-point: five increments). The 625-point design space had measurably smaller best-fit error.

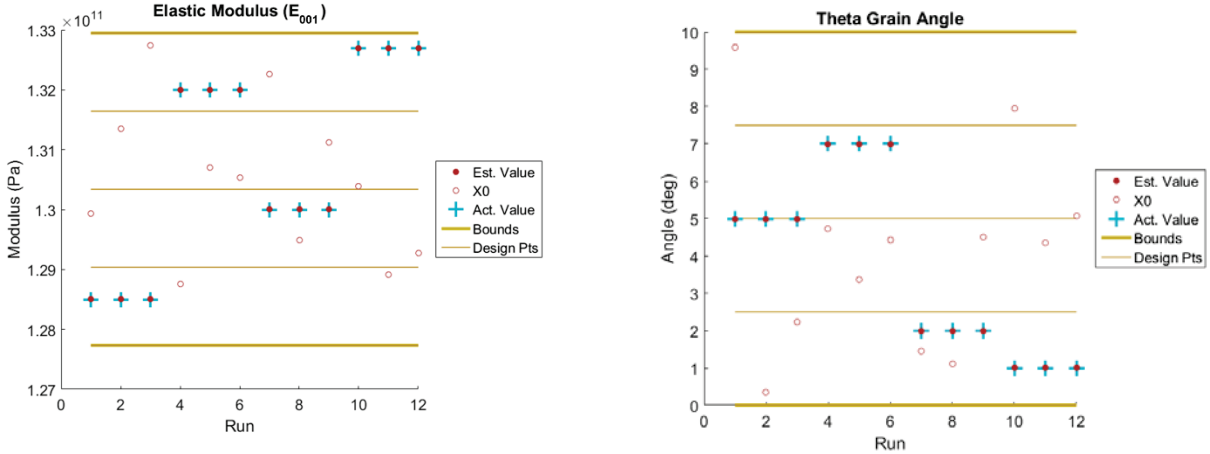

FIGURE 7. FEM-based model inversion interpolated best-fit results for E and θ for parallelepiped SX Mar-M-247 samples.

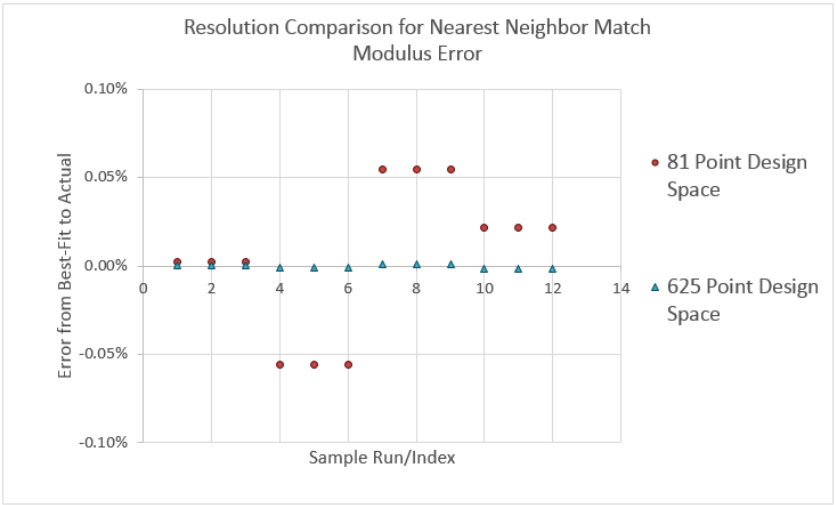

FIGURE 8. Plot of model inversion best-fit error of E_{001} for low (81-point) and medium-resolution (625-point) design spaces.

UNCERTAINTY QUANTIFICATION (UQ)

Uncertainty quantification studies in this paper have applied the UQ process developed in [7] to SX MM247 forward models with geometric, material and damage variation and model inversion of bulk material properties and crystal orientations.

The studies conducted in [7] used Monte Carlo simulations to predict the overall uncertainty on resonance frequency outputs resulting from variation in geometric dimensions, bulk material properties, crystal orientation and creep deformation acting simultaneously. Table 3 shows a list of the parameters included in the Monte Carlo simulations. The one-factor-at-a-time (OFAT) forward model results for all but one of the parameters were used to establish normal distributions within the ranges specified in table 3. The exception was primary grain angle, θ, which used the probability density function defined by Kuo [11] for different levels of casting process control. This study used the Case 2 distribution from [11], with $\alpha = 4$ and $\beta = 1.2$, representing a 'good' casting process control but allowing θ variation to 15 deg. The Monte Carlo simulation script randomly selected a value for each parameter from their respective distributions, and then generated an ANSYS modal simulation for each design point. For the MC3 scenarios in table 3 (MC3, MC3 Creep and MC3 Creep+Cracks), a total of 385 simulations were generated.

TABLE 3. Description of Monte Carlo simulation parameters for SX MM247 dog bone

Name	Design Points	Main Variables	Other Parameters
MC3	150	±2% in *E, ν, A*	4 geometric, θ from 0° to 15°
MC3 Creep	150	±2% in *E, ν, A,* 0.5-8.8% Creep	4 geometric, θ from 0° to 15°
MC3 Creep+Cracks	150	±2% in *E, ν, A,* 0.5-8.8% Creep, 0-20 Cracks	4 geometric, θ from 0° to 15°

A plot of Monte Carlo simulation results is shown in figure 9. The plot quantifies the range of uncertainty in frequency change from the nominal baseline sample with geometry, bulk material properties, crystallographic orientation and creep deformation all accounted for. The inclusion of creep deformation produces an overall decrease in frequencies that corresponds to the OFAT creep changes shown in figure 3. Lower order modes of vibration that tended to show higher sensitivity to creep in figure 3 also tended to have wider uncertainty bounds in figure 9.

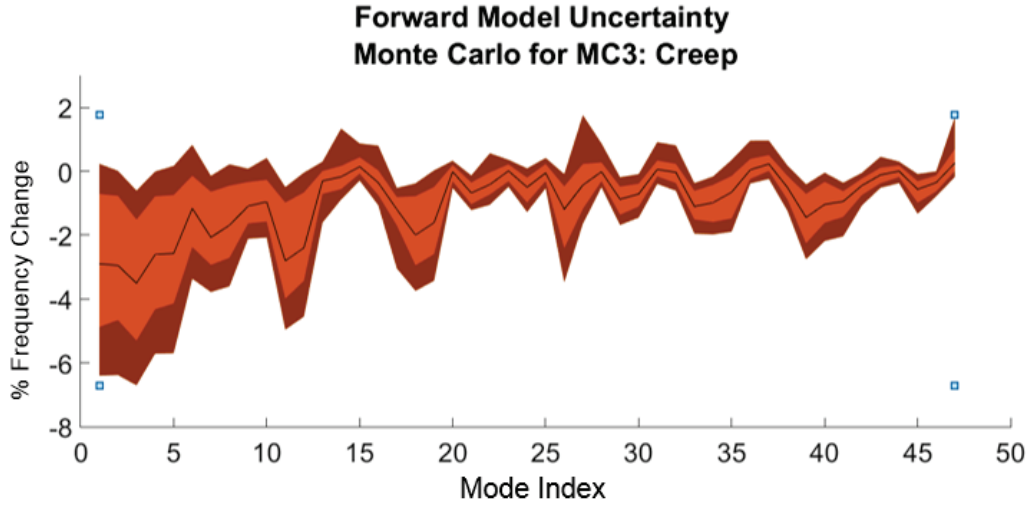

FIGURE 9. Monte Carlo simulation results plot showing uncertainty ranges for MC3 Creep scenario. (Black line: median frequency change from baseline. Light-colored band: 25th to 75 percentile frequency change. Dark colored bands: 10th to 90th percentile frequency change)

One challenge with RUS model-based inversion for a complex part concerns the accuracy of the numerical model. Unfortunately, all FEM models will have some discrepancy with respect to representing real parts under test, for example representing the neck, fillets and threads of a cylindrical dog-bone. Significant model 'residual' error can potentially mask smaller differences due to property variation and lead to greater uncertainty in the inversion results.

A model 'calibration' process is proposed to reduce the residual in the fit between the model and experimental data, and ideally provide greater accuracy in model inversion of sample material state. Most model inversion studies have focused on finding best fit solutions for absolute parameter values such as E_{001}, ν_{001}, A and θ. An example of an inversion residual plot for four SX cylindrical dog-bone specimens are presented in figure 10(a). While quite effective for parts with canonical geometry (like cylinders and parallelepipeds), the root mean square (RMS) error metrics and uncertainty bounds found for complex parts with FEM model have often been larger than desired for an accurate fit. In figure 10(a), the remaining difference in the FEM model is much larger compared to the variation in frequencies between the four test specimens. During the inversion process, with the remaining error dominated by factors not associated with the parameters being estimated, the inversion results will likely be poorer and more prone to local minima. The model calibration approach shows potential for overcoming these limitations by performing a best fit to a select 'reference' part and subsequently inverting material property changes with respect to the standard. For measured data, the reference part is a well-characterized "best known" component in the population. For modeled data, the reference part is set up with nominal values for geometry and material properties. Figure 10(b) and figure 10(c) show the results comparing fit results for absolute parameter values to fit results for a difference from a reference part. The samples are SX MM247 samples from the same casting lot. Fitting to absolute parameter values produces RMS errors in the 0.250 to 0.320 range. Difference fitting produces RMS errors in the 0.019 to 0.150 range, a significant improvement. While promising, further studies for specimen with independently characterized material states are needed to validate this model calibration approach for RUS inversion.

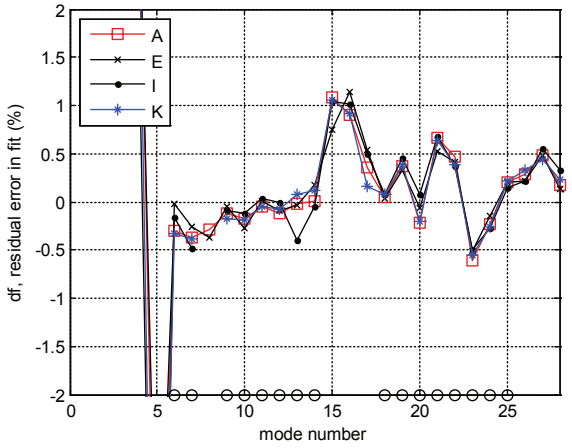

(a)

Specimen	A	E	I	K
E_{001} (Pa)	1.28E+11	1.28E+11	1.28E+11	1.28E+11
ν_{001}	0.377	0.381	0.384	0.379
A	2.83	2.84	2.86	2.83
θ (°)	**5.10**	**6.77**	**4.75**	**4.36**
RMS	**0.317**	**0.258**	**0.312**	**0.312**

(b)

Specimen	A	E	I	K
dE_{001} (%)	0.000	-0.069	-0.502	-0.131
$d\nu_{001}$ (%)	0.000	0.893	0.501	0.000
dA(%)	0.000	0.721	1.65	-0.085
$d\theta$ (°)	**0.000**	**1.58**	**0.59**	**-0.47**
RMS	**0.000**	**0.092**	**0.110**	**0.049**

(c)

FIGURE 10. Model inversion fitting to absolute parameter values (top table) vs. fitting to difference from reference part (68F9A-avg). RMS error from difference fitting is significantly lower that absolute fitting. Crystallographic orientation explains most of the difference between parts

CONCLUSIONS AND FUTURE WORK

Forward modeling, model inversion and uncertainty quantification for PCRT models were studied for several geometries and material states. Forward modeling of SX MM247 dog bones predicted the resonance frequency changes due to creep deformation for a range of creep strains. A virtual PCRT training database was established, and VIPR algorithms were used to generated a PASS/FAIL PCRT sort that could discriminate between acceptable sample design points with geometric and material variation from unacceptable design points with creep strains of 1.0% and greater. The sensitivity of resonance frequencies to variation in macrotexture in Ti-6-4 was investigated. FEM-based model inversion was performed for bulk material property and crystallographic orientation in modeled design points for SX MM247 samples, with excellent interpolated fits for design points. Uncertainty in resonance frequency output in SX MM247 dog bone models was quantified with Monte Carlo simulations that coupled material, geometric, and crystallographic orientation with creep damage. A model calibration process was also developed that evaluates inversion fitting to differences from a designated reference sample rather than absolute property values, yielding a reduction in fit error.

ACKNOWLEDGMENTS

This research was supported by the U.S. Air Force Research Laboratory (AFRL) through a Materials and Manufacturing Director (AFRL/RX) Structural Materials Broad Agency Announcement (BAA) Contract FA8650-15-C-5208 and an AFRL Small Business Innovation Research (SBIR) Phase II Contract, FA8650-15-C-5074. This paper has been cleared for public release by AFRL under case number 88ABW-2016-5410.

REFERENCES

1. Migliori, A., Sarrao, J., Visscher, M. W., Bell, T., Lei, M., Fisk, Z., and Leisure, R., ‘‘Resonant ultrasound spectroscopy techniques for measurement of the elastic moduli of solids,’’ *Physica B*, **183**, 1–24 (1993).
2. Schwarz, J., Saxton, J., and Jauriqui, L., “Process Compensated Resonant Testing in Manufacturing Process Control,” *Material Evaluation*, **63** 736-739, (July 2005).
3. Piotrowski, D., Hunter, L., and Sloan, T., “Process Compensated Resonance Testing JT8D-219 1st Stage Blades,” ATA NDT Forum 2008, (September 24, 2008). [http://www.vibrantndt.co.uk/files/2008_ATA_NDT_Forum-PCRT_of_JT8D-T1_Blades.pdf].
4. Federal Aviation Administration, Atlanta Aircraft Certification Office (2010). A/W File No.: G2010-07 5087.
5. Biedermann, E., Jauriqui, L., Aldrin, J. C., Goodlet, B., Pollock, T., Torbet, C., Mazdiyasni, S., “Resonance Ultrasound Spectroscopy Forward Modeling and Inverse Characterization of Nickel-Based Superalloys,” in *Review of Progress in Quantitative Nondestructive Evaluation,* eds. D.E. Chimenti and L.J. Bond, (American Institute of Physics 1650, Melville NY), **34**, 835-844, (2015).
6. Biedermann, E., Jauriqui, L., Aldrin, J. C., Goodlet, B., Pollock, T., Torbet, C., “Understanding of Resonance Ultrasound Spectroscopy Signature in Precipitate Coarsening of Nickel-Base Superalloy,” AFRL-RX-WP-TR-20140-20237, (2014).
7. Biedermann, E., Jauriqui, L., Aldrin, J. C., Mayes, A., Williams, T., Mazdiyasni, S., “Uncertainty Quantification in Modelng and Measuring Components with Resonant Ultrasound Spectroscopy,” in *Review of Progress in Quantitative Nondestructive Evaluation, Incorporating the 6th European-American Workshop on Reliability of NDE*, eds. D.E. Chimenti and L.J. Bond, (American Institute of Physics, 1706, Melville NY), **35,** 070008_1(1-10 pp) (2016).
8. Goodlet, B. R., Torbet, C. J., Biedermann, E., Jauriqui, L., Aldrin, J. C., Pollock, T. M., “Forward Models for Extending the Mechanical Damage Evaluation Capability of Resonant Ultrasound Spectroscopy,” *Submitted to Ultrasonics*, (2016).
9. Ramaglia, A. D., Villari, P., “Creep and Fatigue of Single Crystal and Directionally Solidified Nickel-base Blades via a Unified Approach Based on Hill48 Potential Function: Part 1 Plasticity and Creep,” *Proceedings of ASME Turbo Expo 2013: Turbine Technical Conference and Exposition.* GT2013-94675. 2013
10. Yang, L., Li, J., Lobkis, O. I., Rokhlin, S. I., “Ultrasonic Propagation and Scattering in Duplex Microstructures with Application to Titanium Alloys,” *Journal of Nondestructive Evaluation,* **31**, 270-283 (2012).
11. Kuo, C. M., “Effects of Disoriented Grains on the Elastic Constants of Directionally Solidified Superalloys,” *Materials Science and Engineering A*, **494**, 103-112 (2008).